Available online at www.sciencedirect.com
SCIENCE DIRECT®
Microelectronic Engineering 77 (2005) 2–7
MICROELECTRONIC ENGINEERING
www.elsevier.com/locate/mee

Fabrication of vacuum tube arrays with a sub-micron dimension using anodic aluminum oxide nano-templates

Sun-Kyu Hwang [a], Soo-Hwan Jeong [b], Ok-Joo Lee [a,c], Kun-Hong Lee [a,*]

[a] *Department of Chemical Engineering, Computer and Electrical Engineering Division, Pohang University of Science and Technology (POSTECH), San-31, Hyoja-Dong, Pohang, Kyungbuk 790-784, Republic of Korea*
[b] *U-team, Samsung Advanced Institute of Technology (SAIT), Suwon 440-600, Republic of Korea*
[c] *Basic Research Laboratory, Electronics and Telecommunications Research Institute, Taejon 305-600, Republic of Korea*

Received 4 May 2004; received in revised form 5 July 2004; accepted 23 July 2004
Available online 21 August 2004

Abstract

Vacuum tube arrays with a sub-micrometer dimension were fabricated by using anodic aluminum oxide (AAO) nano-templates. Ni nanowires deposited electrochemically inside the pores of the AAO nano-templates were used as the field emitters. The pores were sealed by means of angled evaporation of titanium. The field emission measurement was carried out in atmospheric environment outside of a vacuum chamber. The field emission characteristics show low turn-on voltages of 11.0–14.0 V. This phenomenon is attributed to the fact that the distances between the tips of Ni nanowires and the anodes are much smaller than those of conventional designs. Curvature in the Fowler–Nordheim plots at low applied voltage region is due to the variation of the enhanced field at each nanowire tip by the distribution in the length of Ni nanowires.

Keywords: Field emission; Vacuum tube; Anodization; Anodic aluminum oxide

1. Introduction

Vacuum devices based on field emission have attracted considerable attention in recent years because they have several advantages over solid-state devices. They are robust at ambient temperature as well as in radiation environments. They have no power dissipation during electron transport because of the ballistic nature of transport in a vacuum [1]. Consequently, vacuum devices can generate higher power at high frequencies. These characteristics guarantee many applications, including active elements for integrated-circuits,

* Corresponding Author. Tel.: +82 54 279 2271/ 82 562 279 2271; fax : +82 54 279 8298/ 82 562 279 2699.
E-mail address: ce20047@postech.ac.kr (K.-H. Lee).

0167-9317/$ - see front matter © 2004 Elsevier B.V. All rights reserved.
doi:10.1016/j.mee.2004.07.069

flat-panel displays, electron guns, and microwave power tubes [2–4].

Most of the field-emission-based vacuum devices are fabricated by the Spindt process. However, it requires sophisticated processing skills and expensive equipment such as selective etching and electron beam lithography. High voltage is required for the operation of these devices because of the inter-electrode distance of several hundred micrometers. In addition, the Spindt process is difficult to apply to a large area. To overcome these difficulties, we have used anodic aluminum oxide (AAO) technology, which is capable of controlling the dimensions of the structure such as pore diameter, pore length, and pore density with a few nanometer resolution without using electron beam lithography [5–7]. AAO technology can also be easily applied to a large area [8].

In this study, we have fabricated field emitter arrays (FEAs) with integrated anodes by using AAO nano-template. Due to the integrated structure, these vacuum tubes can be operated as stand-alone devices, outside of a vacuum chamber. This work is the basis to devise a novel fabrication process for triode vacuum tube arrays with submicrometer dimensions.

2. Experimental

First, a cleaned and electropolished aluminum sheet of high purity (99.999%) was anodized in

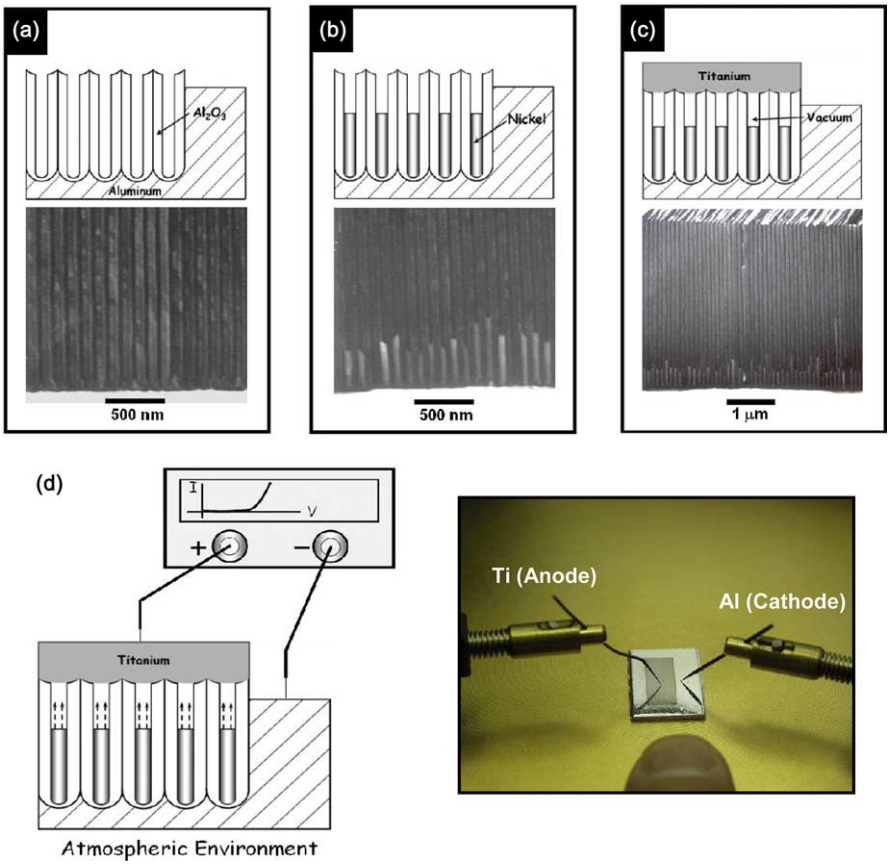

Fig. 1. Fabrication process of integrated diode: (a) AAO template fabrication, (b) electrodeposition of Ni nanowires, (c) angled evaporation of Ti to seal the structure, (d) schematic of a field emission measurement setup.

an oxalic acid solution. After chemically etching the anodized layer in a mixture of chromic acid and phosphoric acid, the second anodization was performed under the same conditions. Details of the fabrication process have been reported elsewhere [9]. Ni nanowires were electrodeposited in the pores of the AAO nano-template. In order to facilitate the growth of Ni nanowires, the voltage was dropped stepwise from 40 to 13 V in 1 V decrements. Subsequent treatment with a phosphoric acid solution widened the pores and thinned the barrier layer simultaneously. Ni nanowires were electrochemically deposited in the pores of the AAO template. The electrodeposition was accomplished in an electrolyte consisting of $NiSO_4 \cdot 6H_2O$ and H_3BO_3 by applying ac voltage. The lengths of Ni nanowires were changed by varying the electrodeposition time. The AAO template containing nickel nanowires was sealed at a pressure of about 10^{-6} torr, using angled evaporation of titanium, which served as an anode of the vacuum tube array.

The morphology and structure of AAO templates and the Ni nanowire were observed by the field emission scanning electron microscope (FE-SEM, Hitachi S-4200) and the transmission electron microscope (TEM, Jeol 1200 EX), respectively. To investigate the chemical composition of the Ni nanowires, energy dispersive X-ray spectrum (EDS) was used. For TEM and EDS investigation, the AAO film was immersed in a 1 M NaOH solution at 80 °C for 6 h. This solution was filtered by using a polycarbonate membrane with a 100 nm pore diameter and rinsed several times with deionized water. The field emission current was measured in atmospheric environment outside of a vacuum chamber as shown in Fig. 1(d) with a diode-type configuration 4155A analyzer (Hewlett–Packard, 4155 A). The remaining aluminum under the AAO template acts as a cathode and the titanium layer on top of the AAO template as an anode. Fig. 1 illustrates the fabrication process in this work.

3. Results and discussion

Fig. 2 shows the progressive change of the surface morphology of a sample. The virgin specimen exhibits surface roughness in μm scale before electropolishing (Fig. 2(a)), but these large surface irregularities are completely removed after electropolishing (Fig. 2(b)). Fig. 2(c) shows the AAO template after 2-step anodization. Pores of an identical dimension are hexagonally closed-packed after the 2-step anodization. The average interpore distance is 110 nm, and the average pore

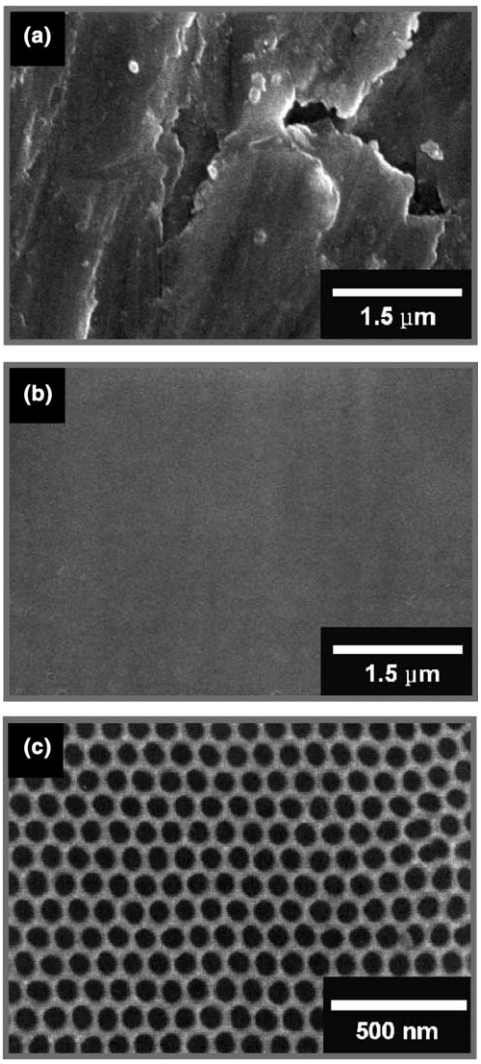

Fig. 2. Change in the surface morphology of a sample throughout the fabrication process. (a) aluminum surface before electropolishing, (b) aluminum surface after electropolishing, (c) AAO template with ordered pore structure obtained after 2-step anodization.

diameter is 70 nm after the pore-widening treatment for 50 min without any change in the surface density of the pores.

Fig. 3 shows the SEM images of the fabricated vacuum tube arrays. The experimental conditions for the preparation of these samples are summarized in Table 1. As shown in Fig. 3, there is a distribution in the lengths of nanowires. This is due to the difference in the thickness of the barrier layer at each pore and due also to the hydrogen evolution caused by water splitting reaction [10]. Ni^{++} ions are reduced during the electrodeposition by the electrons tunneled through the barrier layer. However, the barrier layer at each pore could be branched differently during the barrier layer thinning process, resulting in different energy barriers for tunneling because of different barrier layer thickness [11]. The number of tunneled electrons through an insulating layer decreases exponentially with the thickness of the insulating layer according to Bethe's equation [12]. Consequently, the rate of deposition becomes different at each pore.

Titanium layers were used to seal the pores of the AAO templates. Titanium layers also act as the anodes for vacuum tube arrays. It should be noted that titanium is frequently used as a getter material to maintain the vacuum level in a vacuum device. Infiltration of titanium into the pores must be avoided to prevent short circuits. To achieve this goal, angled evaporation with 20° was performed. It is well known that angled evaporation can prevent the penetration of evaporated metal inside pores [13]. The vacuum degree inside the vacuum device is equal to that of chamber during evaporation.

Fig. 4(a) represents the TEM image of the Ni nanowire fabricated in a pore of an AAO template, and the inset is its electron diffraction pattern. The diameter of the Ni nanowire is about 40 nm. This figure reveals that the diameter of the Ni nanowire is approximately the same as that of the pores in the AAO template. The diffraction pattern is a characteristic one of the well-crystallized metal and is indexed as [1 1 1] reflections with face centered cubic structure (fcc). The chemical, composition of Ni nanowires was investigated by using the EDS. The EDS spectrum of Ni nanowires in Fig. 4(b) shows the peaks of Ni(Lα),

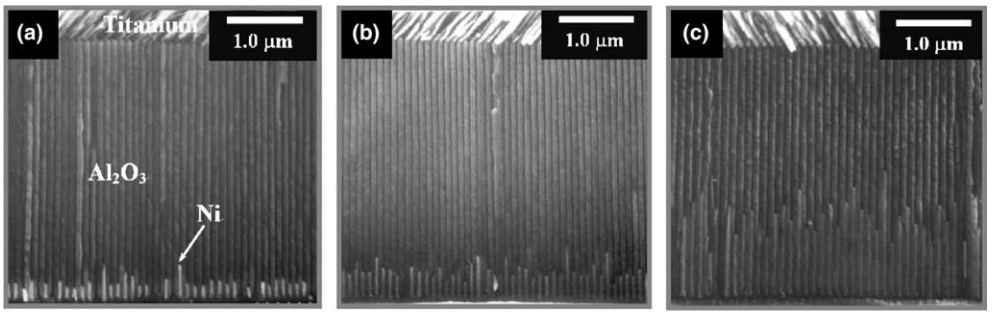

Fig. 3. SEM images of integrated diode structure. Ni nanowires were electrochemically deposited in the pores of the AAO template for (a) 60 s, (b) 150 s, and (c) 270 s.

Table 1
Experimental conditions for three different VTA samples

Sample	Anodizing conditions	Pore widening conditions	Nickel electrodeposition conditions	Anode material
A	2-step anodization 0.3 M oxalic acid 40 V, 15 °C 1st step 12 h 2nd step 30 min	0.1 M phosphoric acid 30 °C 20 min	5 wt% $NiSO_4 \cdot 6H_2O$ + 2 wt% H_3BO_3, 30 °C 18 V_{rms}, 170 Hz 60 s	Titanium
B			5 wt% $NiSO_4 \cdot 6H_2O$ + 2 wt% H_3BO_3, 30 °C 18 V_{rms}, 170 Hz 150 s	Titanium
C			5 wt% $NiSO_4 \cdot 6H_2O$ + 2 wt% H_3BO_3, 30 °C 18 V_{rms}, 170 Hz 270 s	Titanium
D			No deposition	Titanium

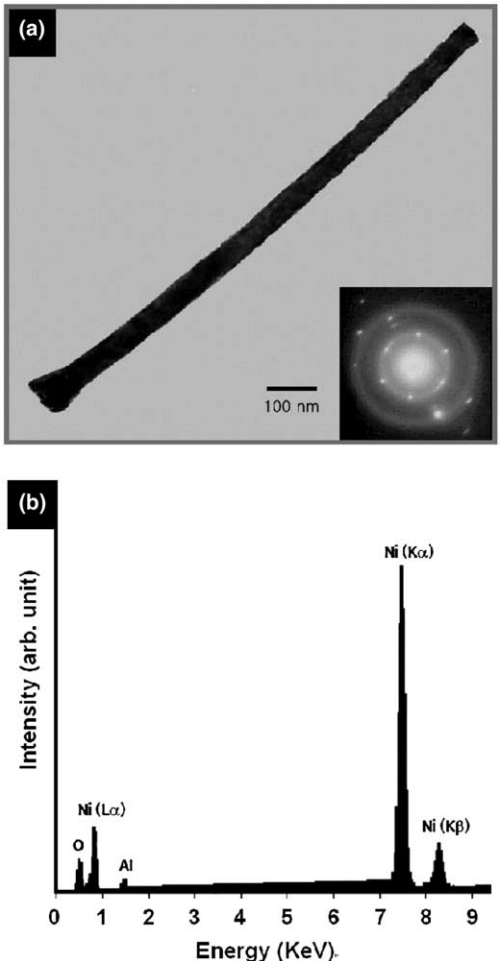

Fig. 4. (a) TEM image of the Ni nanowire. The diameter of Ni nanowire is about 40 nm, the same as that of AAO template. The inset is the electron diffraction pattern for Ni nanowire. Main sharp spots are indexed as [1 1 1] reflections with face centered cubic structure (fcc), (b) Energy dispersive X-ray spectrum of Ni nanowires.

Ni(Kα), and Ni(Kβ), respectively. This reveals that Ni nanowires are made of pure nickel. The small quantity of oxygen and aluminum comes from the residual aluminum oxide not removed completely in sample preparations.

The emission characteristics of the vacuum tube arrays (VTAs) were measured outside of a vacuum chamber. It is possible to measure field emission in an atmospheric condition because of the integrated structure which keeps the vacuum state inside the diode structure. Three different VTAs were fabricated for the field emission measurements. Fig. 5 presents the typical current–voltage relationship of these vacuum tube arrays. A useful parameter for the comparison of the field emission performances of three different samples is the turn-on voltage, V_{to}. The V_{to} values of three samples are found to be 14.0, 12.0, and 11.0 V, respectively. These values are much lower than those values previously reported [14,15]. The distances between the nanowires and the anode (inter-electrode distance) of our samples are less than 3 μm, while those of previous investigators were about several hundred micrometers. Therefore, in our structure, the electric field sufficient for field emission can be supplied to the tips at a low operating voltage. The current–voltage relationship shown in Fig. 5 confirms that the emission current density changes with the inter-electrode distance. As the electrodeposition time increases, the inter-electrode distance decreases. Therefore, specimen C has a larger emission current density than those of other specimens at the same operating voltage. Specimen D is the vacuum tube array without Ni nanowires to measure the magnitude of leakage current. The leakage current between the AAO template cathode and the titanium anode was about 10^{-2} μA/cm^2 at 27 V. As the emission current of the specimen A is 20 μA/cm^2 at the same voltage, the magnitude of leakage current is much smaller than that of the emission current, and might be negligible.

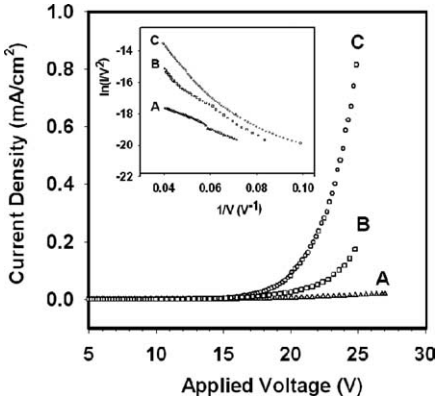

Fig. 5. FE current density vs. applied voltage for integrated diode structure (inset plot) Fowler–Nordheim plots.

Therefore, the currents in Fig. 5 can be considered as the field emission ones.

The inset in Fig. 5 shows the Fowler–Nordheim (FN) plots in our specimens.The emission data of specimen A generally agree with the linear characteristic of the FN relationship corresponding to classical electron tunneling mechanism of field emission, while specimens B and C have substantial curvature at low voltage region in the FN plots. Curvature is expected in the FN plot at very low current and voltage because of the variation in emitter site properties [16]. Levine [17] reported that the substantial curvature in FN plot could be predicted by the statistical distribution of electron emitting sites such as geometrical, structural and electronic characteristics. As shown in Fig. 3(b) and (c), the lengths of Ni emitters in specimens B and C are relatively more distributed than that of specimen A. This means that the enhanced field at each nanowire tip can be distributed due to the variation of distance between each nanowire and anode. Therefore, FN plots of specimens B and C have substantial curvature at low applied voltage and low current region. We estimated the field enhancement factor, β from the slope of the F–N plot. The slope of the F–N plot is equal to $B\varphi^{3/2}d/\beta$, where the constant $B = 6.87 \times 10^9$ V eV$^{-3/2}$ m^{-1}. φ is the work function of the Ni nanowire, and d is the distance between the Ni nanowire and the integrated anode [18]. The work function of the Ni nanowire is assumed to be the same as the bulk nickel having [1 1 1] plane (=5.35 eV). Field enhancement factors for A, B, and C were calculated using the above equation, and were in the range of 560–2790. Because FN plots have different slopes at low voltage and high voltage regions in specimens B and C, β values are expressed by range. These low β values may result from the field screening effect by the high nanowire density of about 10^{10} tips/cm^2 [19].

4. Conclusion

We have fabricated vacuum tube arrays with a sub-micrometer dimension by using AAO nanotemplates. Current–voltage characteristics show low turn-on voltages of 11.0–14.0 V. This phenomenon is attributed to the fact that the distances between the tips of Ni nanowires and the anodes are much smaller than those of conventional designs. Curvature in the FN plots at low applied voltage region is due to the variation of enhanced field at each nanowire tip by the distribution in the length of Ni nanowires.

Acknowledgements

This work was supported by the National R&D Project for Nano Science and Technology and by the Brain Korea 21 Project in 2003.

References

[1] I. Brodie, P.R. Schwoebel, Proc. IEEE 82 (1994) 7.
[2] I. Brodie, IEEE Trans. Electron. Dev. 36 (1989) 2641.
[3] R. Meyer, A. Ghis, P. Rambaud, F. Müller, Proc. Jpn. Display (1985) 513.
[4] P. Chang, D. Kern, L. Muray, IEEE Trans. Electron. Dev. 38 (1991) 2284.
[5] H. Masuda, K. Fukuda, Science 268 (1995) 1466.
[6] A.P. Li, F. Müller, A. Birner, K. Nielsch, U. Gösele, J. Appl. Phys. 84 (1998) 6023.
[7] S. Shingubara, O. Okino, Y. Sayama, H. Sakaue, T. Takahagi, Jpn. J. Appl. Phys. 36 (1997) 7791.
[8] H. Masuda, H. Yamada, M. Satoh, H. Asoh, Appl. Phys. Lett. 71 (1997) 2770.
[9] S.-K. Hwang, S.-H. Jeong, H.-Y. Hwang, O.-J. Lee, K.-H. Lee, Korean J. Chem. Eng. 19 (2002) 467.
[10] W. Sautter, G. Ibe, J. Meier, Aluminium 50 (1974) 143.
[11] Y.C. Sui, B.Z. Cui, L. Martínez, R. Perez, D.J. Sellmyer, Thin Solid Films 406 (2002) 64.
[12] E.E. Polymeropoulos, J. Appl. Phys. 48 (1977) 2404.
[13] A.A.G. Driskill-Smith, D.G. Hasko, A. Ahmed, Appl. Phys. Lett. 75 (1999) 2845.
[14] D.N. Davydov, P.A. Sattari, D. Almawlawi, A. Osika, T.L. Haslett, J. Appl. Phys. 86 (1999) 3983.
[15] A.N. Govyadinov, S.A. Zakhvitcevich, J. Vac. Sci. Technol. B 16 (1998) 1222.
[16] A.N. Obraztsov, Al.A. Zakhidov, A.P. Volkov, D.A. Lyashenko, Microelectron Eng. 69 (2003) 405.
[17] J.D. Levine, J. Vac. Sci. Technol. B 13 (1995) 553.
[18] J.-M. Bonard, J.-P. Salvetat, T. Stöckli, L. Forró, A. Châtelain, Appl. Phys. A 69 (1999) 245.
[19] D.N. Davydov, P.A. Sattari, D. AlMawlawi, A. Osika, T.L. Haslett, M. Moskovits, J. Appl. Phys. 86 (1999) 3983.